ACS OMEGA

Open Access

http://pubs.acs.org/journal/acsodf

Article

Novel Penicillin-Based Sulfone-Siderophore Conjugates for Restoring β-Lactam Antibiotic Efficacy

Diana Rodríguez, Emilio Lence, Juan C. Vázquez-Ucha, Alejandro Beceiro, and Concepción González-Bello*

Cite This: *ACS Omega* 2024, 9, 26484−26494

Read Online

ACCESS | Metrics & More | Article Recommendations | Supporting Information

ABSTRACT: Membrane permeability is a natural defense barrier that contributes to increased bacterial drug resistance, particularly for Gram-negative pathogens. As such, accurate delivery of the antibacterial agent to the target has become a growing research area in the infectious diseases field as a means of improving drug efficacy. Although the efficient transport of siderophore-antibiotic conjugates into the cytosol still remains challenging, great success has been achieved in the delivery of β-lactam antibiotics into the periplasmic space via bacterial iron uptake pathways. Cefiderocol, the first siderophore-cephalosporin conjugate approved by the US Food and Drug Administration, is a good example. These conjugation strategies have also been applied to the precise delivery of β-lactamase inhibitors, such as penicillin-based sulfone **1**, to restore β-lactam antibiotic efficacy in multidrug-resistant bacteria. Herein, we have explored the impact on the bacterial activity of **1** by modifying its iron chelator moiety. A set of derivatives functionalized with diverse iron chelator groups and linkages to the scaffold (compounds **2**−**8**) were synthesized and assayed in vitro. The results on the ability of derivatives **2**−**8** to recover β-lactam antibiotic efficacy in difficult-to-treat pathogens that produce various β-lactamase enzymes, along with kinetic studies with the isolated enzymes, allowed us to identify compound **2**, a novel β-lactamase inhibitor with an expanded spectrum of activity. Molecular dynamics simulation studies provided us with further information regarding the molecular basis of the relative inhibitory properties of the most relevant compound described herein.

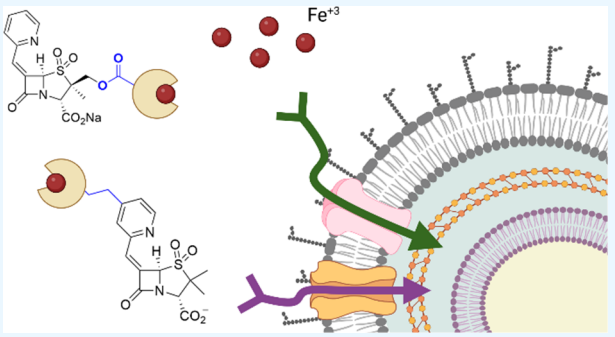

INTRODUCTION

The ever-increasing emergence and worldwide spread of new and more sophisticated bacterial resistance mechanisms to elude the action of current antibiotics are threatening our ability to treat infectious diseases.[1] This scenario makes infections caused by bacterial pathogens that are resistant to multiple types of antibiotics a global health challenge of unknown proportions.[2] Bacterial resistance mechanisms, such as hydrolysis of the antibiotic by β-lactamase enzymes, modifications to the bacterial target, or drug excretion by the activation of efflux pumps, are among the factors contributing to the innate resistance of bacteria to antibiotics.[3] To curb this worrying trend, the strategies pursued widely in recent years are directed to addressing infections without damaging microbiome stability or incentivizing bacterial resistance.[4] To this end, huge efforts have been devoted to developing (i) narrow-spectrum antibiotics that specifically kill the pathogen[5] and (ii) β-lactamase inhibitors that are able to reduce the impact of the main bacterial resistance mechanism in the critical priority pathogens *Pseudomonas aeruginosa*, *Acinetobacter baumannii*, and Enterobacterales, namely, hydrolysis of β-lactam antibiotics catalyzed by β-lactamase enzymes.[6] The latter approach, which is receiving great attention from the pharmaceutical industry, is the main strategy currently available for restoring the effectiveness of β-lactam antibiotics, which represent about 70% of all antibiotics prescribed.

Since membrane permeability is a bacterial natural defense barrier that also contributes to enhancing drug resistance, especially for Gram-negative pathogens, accurate delivery of the antibacterial agent to the target (inside the bacterium) has become a growing research area in the infectious diseases field to enhance drug efficacy. The main issue of drug internalization is to combine, in a single chemical entity, the molecular requirements for efficient interaction with the target (polar functional groups, global charge of the compound, etc.) as well as with the bacterial cell wall, which is particularly complex for Gram-negative bacteria. Inspired by the bacterial iron acquisition mechanism to uptake insoluble Fe(III) from environmental stocks of the host to meet the needs for this

Received: March 28, 2024
Revised: May 13, 2024
Accepted: May 17, 2024
Published: May 28, 2024

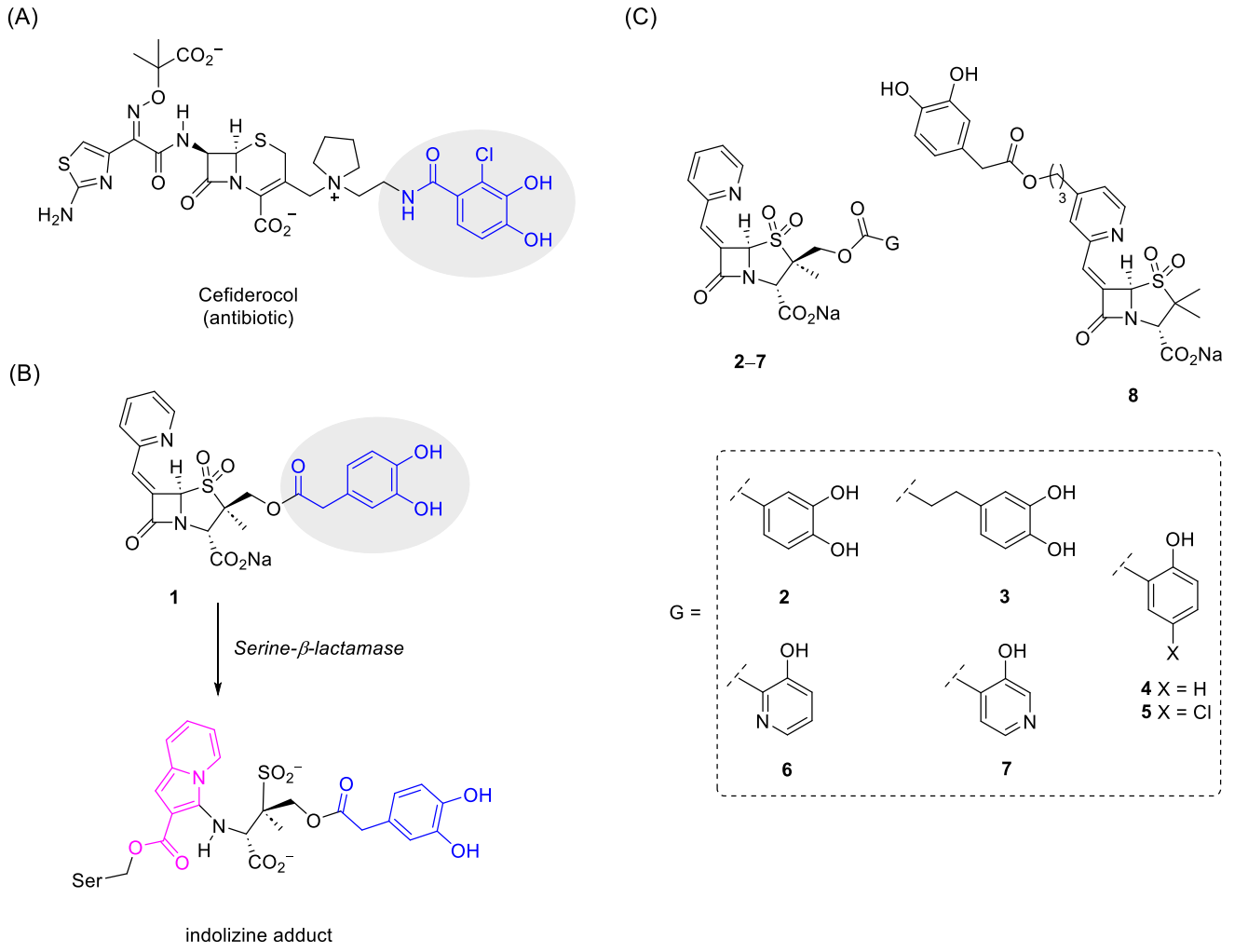

Figure 1. (A) Chemical structure of cefiderocol, the first siderophore-cephalosporin conjugate approved by the FDA (2019). (B) Inhibition mechanism of compound **1** (LN-1−255) against serine-β-lactamase enzymes. (C) Target compounds **2**−**8**.

essential nutrient, siderophore-antibiotic conjugate-based approaches have been developed recently.[7−11] Bacteria use iron chelator (siderophore) groups that have high affinity and specificity for Fe(III) to form stable and water-soluble Fe(III)-complexes, which are then taken up by ferric-chelate-specific transporters into the cell. Although the efficient transport of siderophore-antibiotic conjugates into the cytosol still remains challenging, great success has been achieved in the delivery of β-lactam antibiotics into the periplasmic space. Cefiderocol (formerly S-649266), the first siderophore-cephalosporin conjugate approved in late 2019 by the US FDA (Food and Drug Administration), is a good example (Figure 1A).[12−19]

The siderophore conjugation strategy has also been applied to deliver the β-lactamase inhibitor **1** (LN-1−255) into the periplasmic space (Figure 1B). This compound, which was developed by Buynak,[20−22] has been shown to have an outstanding activity against bacterial species carrying the challenging and hard-to-inhibit carbapenem-hydrolyzing class D β-lactamases to restore carbapenem activity.[23,24] These β-lactamases are widely dispersed in clinically relevant species such as *A. baumannii* (OXA-23 or OXA-24/40) or Enterobacterales (OXA-48) and are critically limiting the use of carbapenems, which in many cases are the last option available. When compound **1** binds to the enzyme active site, it undergoes a nucleophilic attack by the catalytic serine residue to generate an indolizine adduct, which is stable against hydrolysis. This reactivity of the (2-pyridyl)methylene group was found by researchers from Pfizer in 1986 when this moiety was incorporated at C6 of the sulbactam to increase its efficacy against β-lactamases from *S. aureus* and *E. coli* (micromolar).[25] The authors demonstrated the formation of the indolizine derivative by reaction with sodium methoxide. The resulting indolizine ester increases the hydrophobicity of the hydrophobic region near the active site, thus preventing the attack of the water molecule required to restore enzymatic activity.[26] The available crystallographic structure of SHV-1 from *K. pneumoniae* covalently modified by **1** (PDB ID 3D4F, 1.55 Å), in which the indolizine adduct was also identified, reveals that the siderophore moiety does not seem to contribute significantly to the binding.[21] Thus, a large variability in the conformations of the side chain containing the catechol group, with differences of more than 10 Å, is seen, and it also points toward different pockets of the enzyme active site.

In this work, we have explored the impact on the ability of **1** to restore β-lactam antibiotic efficacy in multidrug-resistant bacteria, by modifying (i) the length of the spacer connecting the catechol group and the 6-pyridylmethylene penicillin-based sulfone scaffold (compounds **2**−**3**), through which its strength against hydrolysis is also modified (aliphatic vs aromatic esters); (ii) replacement of the catechol group in the pro-*S*

https://doi.org/10.1021/acsomega.4c02984
ACS Omega 2024, 9, 26484−26494

methyl group by another type of the iron chelator group (compounds **4**−**7**);[27−30] and (iii) introduction of the catechol group in the pyridyl moiety (compound **8**) (Figure 1C). In vitro studies on the ability of derivatives **2**−**8** to recover β-lactam antibiotic efficacy in difficult-to-treat pathogens harboring extended spectrum β-lactamases (ESBL) of classes A and C and carbapenem-hydrolyzing class D β-lactamases led us to identify compound **2**, which improves the in vitro activity of **1** against CTX-M-14 ESBL-producing *E. coli* and OXA-48 carbapenemase-producing *K. pneumoniae*. Kinetic studies on the most relevant compounds reported herein with isolated β-lactamases, along with molecular dynamics (MD) simulation studies, allowed us to provide further insights into the molecular basis of its inhibitory properties.

RESULTS AND DISCUSSION

Synthesis of Compounds 2−8. Target compounds **2**−**7** were synthesized from sulfone **10**, which was prepared according to modified previously reported protocols, in eight steps from commercially available (+)-6-aminopenicillanic acid (Figure 2).[23] The synthetic approach involves replacement of the 2-chloroacetyl moiety in **10** by the arylacyl groups in compounds **11**−**16**, followed by removal of the protecting groups.

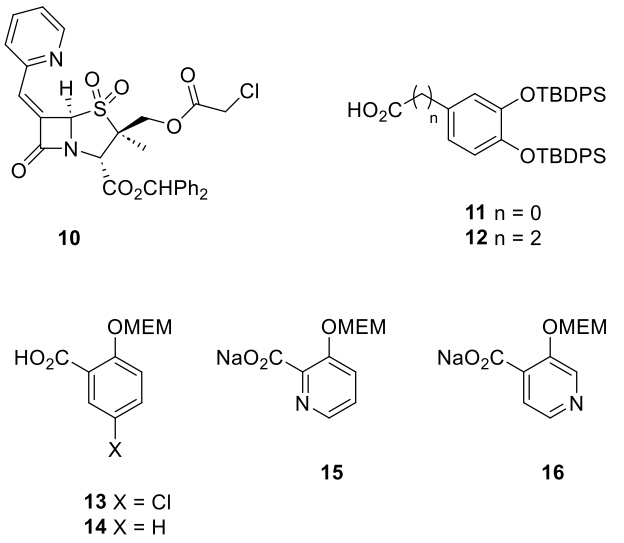

Figure 2. Key intermediates in the synthesis of target compounds **2**−**7**.

First, the required protected catechols **11**−**12** were synthesized in two steps from 3,4-dihydroxybenzoic (**17**) and 3-(3,4-dihydroxyphenyl)propanoic acid (**18**), respectively, both of which are commercially available (Scheme 1). Thus, treatment of catechols **17** and **18** with *tert*-butyldiphenylsilane chloride and imidazole provided protection of the phenol groups, such as **19**, together with the carboxylic acids, which, upon treatment with lithium hydroxide, followed by acidification with dilute HCl, gave the desired acids **11** and **12**. Protection of the phenol group in commercially available methyl esters **20** and **21** with 2-methoxyethoxymethyl chloride using sodium hydride as a base gave MEM ethers **22** and **23**, which were transformed into acids **13** and **14**, respectively, in excellent yields by hydrolysis. Following the same protocol methyl esters **24** and **26** were transformed into targeted siderophores **15** and **16**, respectively. However, as we had

Scheme 1. Synthesis of Compounds 11−16[a]

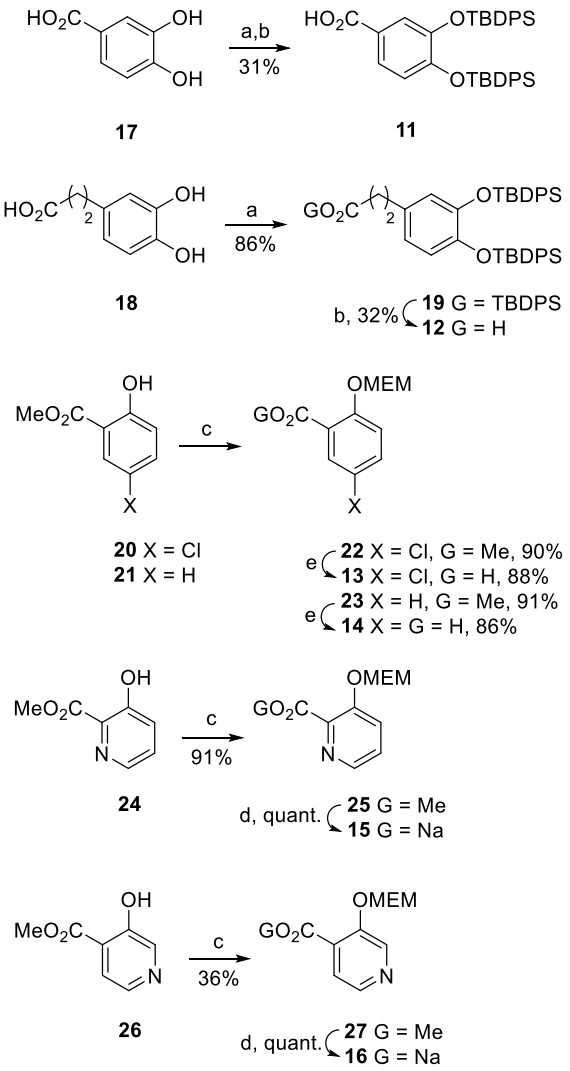

[a]Reagents and conditions: (a) TBDPSCl, imidazole, DMF, RT. (b) 1. LiOH, THF, RT. 2. HCl (aq.). (c) 1. NaH, THF, 0 °C. 2. MEMCl, 0 °C → RT. (d) NaOH (1 M), MeOH, RT. (e) 1. NaOH (1 M), MeOH, Δ. 2. HCl (1 M).

observed that acidification with dilute HCl during workup caused deprotection of the MEM group, the corresponding sodium salts were employed.

Next, removal of the 2-chloroacetyl group in compound **10** by treatment with thiourea in the presence of pyridine provided the desired primary alcohol for introduction of the siderophore group (Scheme 2). Thus, treatment of the latter compound with *N*-(3-(dimethylamino)propyl)-*N*′-ethylcarbodiimide, 4-*N*,*N*-dimethylaminopyridine and the acids **11**−**14**, and the sodium salts **15** and **16** gave rise to esters **28**−**31** and **36**−**37** in isolated yields ranging from 45 to 66%. Deprotection of the MEM groups in ethers **28**−**31** by heating in *tert*-butanol in the presence of pyridinium 4-toluenesulfonate gave phenols **32**−**35** with isolated yields ranging from 49 to 68%. On the other hand, the treatment of derivatives **36**−**37** with tetrabutylammonium fluoride and acetic acid led to catechols **38** and **39** in 57 and 68% yields, respectively. Finally, benzhydryl esters **32**−**35** and **38**−**39** were converted into derivatives **2**−**7** by heating with *m*-cresol followed by

https://doi.org/10.1021/acsomega.4c02984
ACS Omega 2024, 9, 26484−26494

Scheme 2. Synthesis of Compounds 2−7

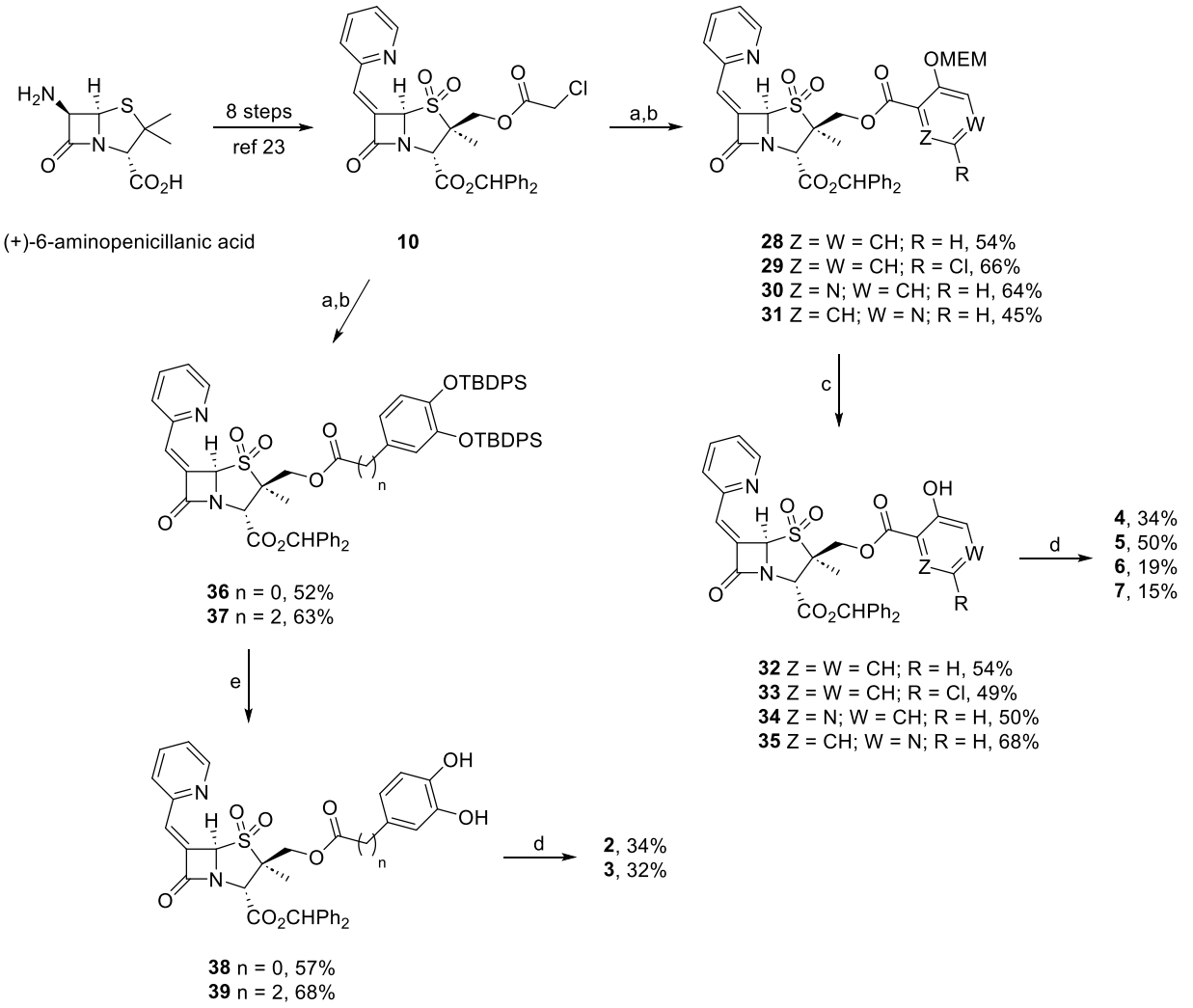

[a]Reagents and conditions: (a) Thiourea, Py, DMF, 0 °C → RT. (b) **11**−**16**, EDC, DMAP, DCM, −15 °C → RT. (c) Pyridinium 4-toluenesulfonate, *t*-BuOH, RT. (d) 1. *m*-cresol, 50 °C. 2. $NaHCO_3$. (e) TBAF, AcOH, THF, 0 °C → RT.

neutralization with sodium bicarbonate (isolated yields ranging from 15 to 50%).

Compound **8** was synthesized following the sequence of reactions indicated in Scheme 3. The key step involved introduction of the siderophore-functionalized pyridylmethylidene group by means of a Wittig reaction between ketone **47**, which is readily obtained by the oxidation of position C6 in the previously described benzhydryl 6-aminopenicylate (**46**),[31] and the phosphonium salt **45**. Compound **45** was prepared in six steps from commercially available 4-bromo-2-methylpyridine (**40**) (Scheme 3). First, following previously described procedures, the Heck-type cross-coupling reaction between bromide **40** and ethyl acrylate, using palladium(II) acetate as the catalyst and tri*o*-tolylphosphine as the ligand, yielded ethyl (*E*)-3-(2-methylpyridin-4-yl)acrylate (**41**) in an isolated yield of 92%. Full reduction of the *α*,*β*-unsaturated ester **41** by treatment with sodium borohydride in the presence of methanol led to the primary alcohol **42** in an isolated yield of 91%, which was protected by treatment with *tert*-butyldiphenylsilane chloride in the presence of imidazole, to give rise to compound **43** quantitatively. Subsequently, benzylic oxidation of the methyl group in **43** by formation of the corresponding *N*-oxide by treatment with *m*-chloroperbenzoic acid, followed by acetalization and subsequent basic hydrolysis, turned out to be unselective. A chromatographically inseparable mixture of alcohols resulting from oxidation of the two benzylic positions in **43** was obtained. Subsequent Appel reaction of the latter mixture by treatment with triphenylphosphine and carbon tetrabromide gave bromide **44** in an overall isolated yield of 28% from **43**. Finally, bromide **44** was converted to the phosphonium salt **45** by heating with triphenylphosphine (74% yield).

Next, ketone **47** was prepared from amine **46**[36] by treatment with triflic anhydride and triethylamine followed by treatment with dilute HCl. Wittig reaction between ketone **47** and the ylide derivative of phosphonium salt **45** gave compound **48** in an overall isolated yield of 40% (Scheme 3). Oxidation of sulfide **48** with *m*-chloroperbenzoic acid gave sulfone **49** in an isolated yield of 76%. TBDPS-deprotection in **49** by treatment with tetrabutylammonium fluoride and acetic acid gave primary alcohol **50** (89% yield). Esterification of alcohol **50** with acid **51**[23] using EDC (*N*-(3-(dimethylamino)propyl)-*N*′-ethylcarbodiimide), in the presence of 4-*N*,*N*-dimethylaminopyridine, led to ester **52** in an isolated yield of 71%. Finally,

https://doi.org/10.1021/acsomega.4c02984
ACS Omega 2024, 9, 26484−26494

Scheme 3. Synthesis of Compound 8[a]

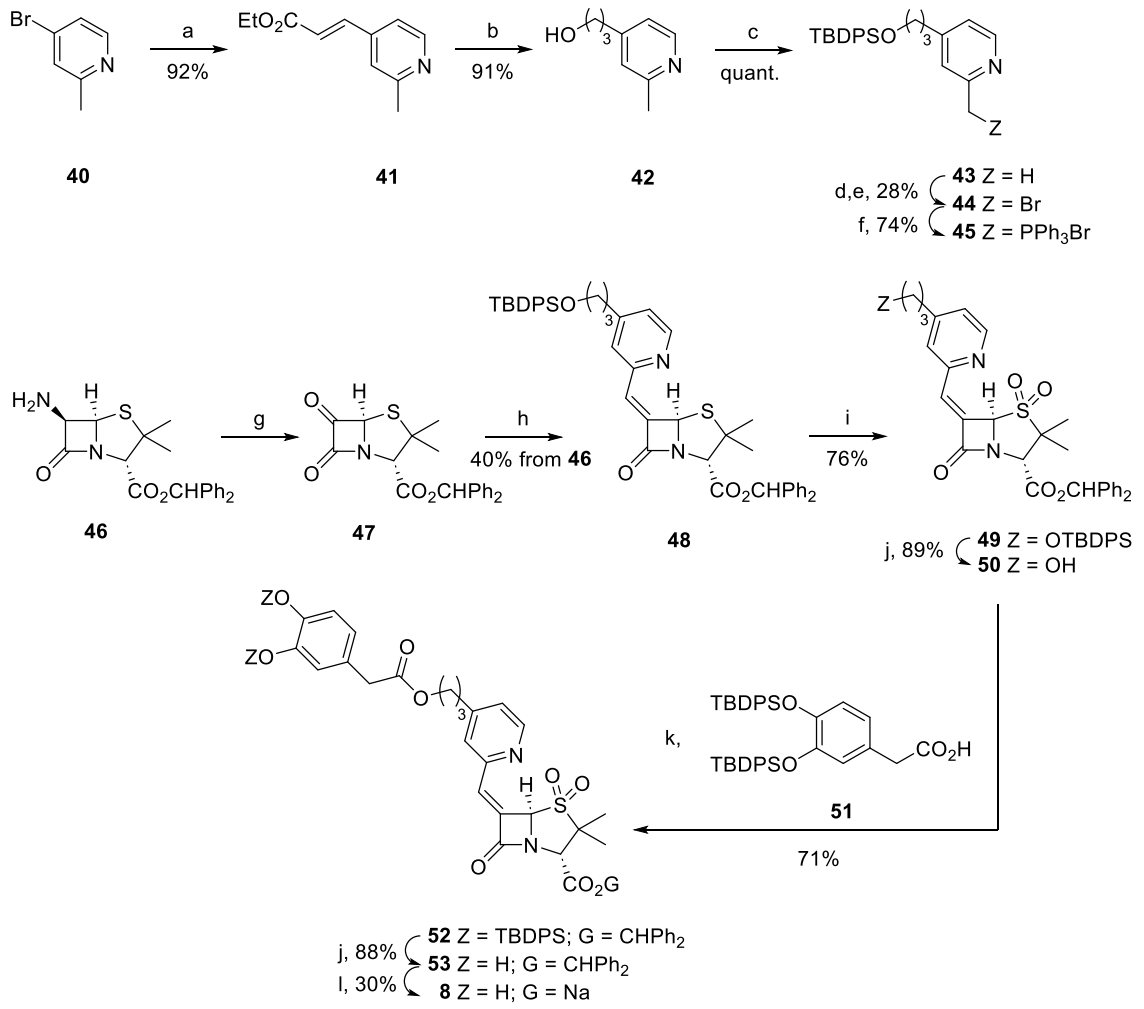

[a]Reagents and conditions: (a) Ethyl acrylate, $Pd(OAc)_2$, P(*o*-tol)$_3$, Et_3N, DMF, 100 °C. (b) $NaBH_4$, MeOH, 0 °C → 80 °C. (c) TBDPSCl, imidazole, DMF, RT. (d) 1. *m*-CPBA, $CHCl_3$, RT. 2. Ac_2O, 90 °C. 3. KOH, MeOH, 0 °C → RT. (e) CBr_4, Ph_3P, CH_2Cl_2, 0 °C. (f) Ph_3P, PhMe, Δ. (g) 1. Tf_2O, Et_3N, CH_2Cl_2, −78 °C → 0 °C. 2. Et_3N,−78 °C. 3. HCl (0.5 M), −78 °C → RT. (h) 1. **45**, *t*BuOK, THF, RT. 2. **47**, CH_2Cl_2, −78 °C. (i) *m*-CPBA, DCM, t.a. (j) TBAF, AcOH, THF, 0 °C. (k) **51**, EDC, DMAP, DCM, −15 °C → RT. (l) 1. *m*-cresol, 50 °C. 2. $NaHCO_3$ (aq.).

benzhydryl ester **52** was transformed in two steps into the target compound **8** as compounds **2**−**3** from **36**−**37**.

In Vitro Activity and Enzymatic Studies. The ability of compounds **2**−**8** to restore *β*-lactam antibiotic activity in four different pathogens (*Escherichia coli*, *Klebsiella pneumoniae*, *Pseudomonas aeruginosa*, and *Acinetobacter baumannii*) producing diverse types of serine-*β*-lactamase enzymes was measured and compared with the parent compound **1** and avibactam. Bacterial strains harboring the following *β*-lactamase enzymes were employed: (i) extended spectrum *β*-lactamases (ESBL) of classes A (CTX-M-14) and classes C (CMY-2, DHA-1, FOX-4, and PDC-1) and (ii) carbapenem-hydrolyzing class D *β*-lactamases (OXA-23, OXA-24/40, and OXA-48) (Table S1). The minimum inhibitory concentration (MIC) of each antibiotic (ampicillin, ceftazidime, and imipenem) and antibiotic/compound combinations were determined using the broth microdilution method and following CLSI (Clinical and Laboratory Standards Institute) criteria.[32] MIC was defined as the lowest concentration of antibiotic or antibiotic/compound combination inhibited visible growth of the microorganism after 20 h of incubation at 37 °C. Assays were performed at a concentration of 16 $\mu g\ mL^{-1}$. The results, which are the mean values of three independent replicates, are summarized in Table 1. Compounds **1**−**8** did not show intrinsic antibacterial activity.

The results of comparative MIC assays for ampicillin, ceftazidime, and imipenem, in combination with the compounds reported herein, revealed that linkage of the catechol group to the pro-*S* methyl of the penicillin-based sulfone scaffold via an aromatic ester group (compound **2**) provided better results than using aliphatic esters, such as for **3** or **1**, since the spectrum of activity of inhibitor **2** was expanded. Thus, in comparison with the parent compound **1**, the susceptibility of imipenem and ampicillin in combination with **2** against *K. pneumoniae* carrying carbapenemases OXA-48 and *E. coli* producing ESBL CTX-M-14 was increased by 2- and 4-fold, respectively. For the other resistant bacterial strains studied herein, the in vitro activity of the antibiotic in combination with **2** was retained since the same MIC values were obtained as for the combination with **1**. Except for the *E. coli* strain harboring the ESBL CTX-M-14, the activity of the antibiotic was fully restored in the presence of compound **2**, affording low MIC values. Specifically, MIC values of between ≤0.06 and ≤1 $\mu g\ mL^{-1}$ for *E. coli* strains, 0.5 $\mu g\ mL^{-1}$ for *A.*

https://doi.org/10.1021/acsomega.4c02984
ACS Omega 2024, 9, 26484−26494

Table 1. MIC Values (μg mL^{-1}) for Ampicillin, Ceftazidime, and Imipenem with Several Bacterial Strains Carrying Representative β-Lactamases of Classes A (CTX-M-14), C (CTX-M-2, CMY-2, DHA-1, FOX-4, and PDC-1), and D (OXA-23, OXA-24/40, and OXA-48) in the Presence and Absence of β-Lactamase Inhibitors 1−8 and Avibactam[a]

	Class A		Class C				Class D		
	CTX-M-14	CTX-M-2	CMY-2	DHA-1	FOX-4	PDC-1	OXA-23	OXA-24/40	OXA-48
bacterial strain and type of β-lactamase produced	*E. coli* MG1655 + pBGS18 + CTX-M-14	*E. coli* MG1655 + pBGS18 + CTX-M-2	*E. coli* TG1 + pBGS18 + CMY-2	*E. coli* TG1 + pBGS18 + DHA-1	*E. coli* TG1 + pBGS18 + FOX-4	*P. aeruginosa* PAO Δ*ampD*	*A. baumannii* ATCC 17978 + pET-RA-KmR + OXA-23	*A. baumannii* ATCC 17978 + pET-RA-KmR + OXA-24/40	*K. pneumoniae* ΔompK35/36+ pBGS18+ OXA-48
spectrum of β-lactamase activity	ESBL	ESBL	ESBL	ESBL	ESBL	ESBL	carbapenemase	carbapenemase	carbapenemase
antibiotic used	AMP	CAZ	CAZ	CAZ	CAZ	CAZ	IP	IP	IP
without an inhibitor	1024	1024	16	32	>64	8	8	64	64
avibactam	NA	NA	NA	NA	NA	1	4	16	NA
1	16	≤1	≤0.06	≤0.06	≤0.06	1	0.5	0.5	4
2	4	≤1	≤0.06	≤0.06	≤0.06	1	0.5	0.5	2
3	32	2	≤0.06	≤0.06	0.12	1	0.5	1	16
4	256	64	0.12	0.25	2	2	2	16	16
5	512	64	0.12	0.12	16	2	2	16	16
6	1024	512	4	16	32	8	8	64	64
7	1024	256	1	4	0.12	4	4	32	16
8	1024	256	4	8	8	8	4	32	32
without β-lactamase	2	2	≤0.06	≤0.06	≤0.06	1	0.5	0.5	0.5

[a]Inhibitor concentration = 16 μg mL^{-1}; AMP = ampicillin; CAZ = ceftazidime; IP = imipenem; NA = not applicable (avibactam shows antimicrobial activity against these strains); yellow shadow = susceptibility increased relative to **1**; blue shadow = susceptibility maintained relative to **1**.

Table 2. Inhibition Kinetics of OXA-23, OXA-48, and PDC-1 by Compounds 1, 2, and 9 and Avibactam[a]

enzyme	inhibitor	IC_{50} (μM)	K_{iapp} (μM)	K_I (μM)	k_{inact} (s^{-1})	k_{inact}/K_I (M^{-1} s^{-1})
OXA-23	**1**	0.012 ± 0.008	0.088 ± 0.006	0.30 ± 0.08	0.041 ± 0.005	$1.4 \times 10^5 \pm 0.3 \times 10^5$
	2	0.051 ± 0.012	0.817 ± 0.274	0.716 ± 0.061	0.040 ± 0.002	$5.7 \times 10^4 \pm 0.5 \times 10^4$
	AVI	8.93 ± 0.99	105.56 ± 3.08	203.93 ± 22.6	0.057 ± 0.009	$2.9 \times 10^3 \pm 0.6 \times 10^3$
OXA-48	**1**	0.003 ± 0.0003	0.17 ± 0.01	ND	ND	ND
	2	0.013 ± 0.002	0.045 ± 0.007	0.131 ± 0.011	0.045 ± 0.004	$3.4 \times 10^5 \pm 0.3 \times 10^5$
	AVI	0.852 ± 0.051	9.830 ± 2.612	38.918 ± 14.601	0.086 ± 0.010	$2.4 \times 10^3 \pm 0.8 \times 10^3$
PDC-1	**1**	0.0061 ± 0.0019	0.053 ± 0.019	0.0748 ± 0.0189	0.046 ± 0.006	$6.3 \times 10^5 \pm 1.4 \times 10^5$
	2	0.0013 ± 0.0002	0.005 ± 0.001	0.0113 ± 0.0019	0.032 ± 0.005	$2.9 \times 10^6 \pm 0.8 \times 10^6$
	AVI	0.0510 ± 0.0031	0.990 ± 0.075	ND	ND	ND

[a]ND = not determined because the maximum k_{obs} required to calculate the parameter was not reached; AVI = avibactam.

baumannii, and 1 μg mL^{-1} for *P. aeruginosa* were obtained. Moreover, among the iron chelator groups introduced at the pro-*S* methyl moiety of the scaffold (compounds **2**−**7**), the catechol group proved to be the most efficient as regards internalization into the periplasmic space (compounds **2**−**3**) as replacement by the phenol groups in compounds **4**, **5**, **6**, and **7** decreased the susceptibility of the antibiotics against the strains studied. Importantly, the results with compound **8**, which contains the catechol group in position 4 of the pyridyl moiety, show low effectiveness in restoring the antibiotic activity, thus indicating the need to incorporate it into the pro-*S* methyl group of the 6-pyridymethylene penicillin-based sulfone.

Taken together, the reported susceptibility studies revealed that compound **2** restores the antibacterial activity of imipenem, ceftazidime, and ampicillin against the bacterial strains studied, thereby expanding its spectrum of activity. To demonstrate that the penicillin-based sulfones reported herein are inhibitors of the β-lactamase enzymes produced by the pathogens studied, the inhibitory capacity of the most relevant compound identified in this work, namely, compound **2**, against carbapenemases OXA-23 and OXA-48 and the ESBL PDC-1 was determined. Enzyme purifications and the kinetic parameters IC_{50}, inhibition constant (K_I), apparent inhibition constant (K_{iapp}), inactivation rate (k_{inact}), and inhibition efficiency (k_{inact}/K_I), were calculated in the presence of nitrocefin (reported substrate) following previously described protocols.[33,34,24] The data, which are the mean values (and standard deviation) of triplicate samples, are summarized in Table 2. The activity of aromatic esters **4**, **5**, and **6** was also determined against the OXA-24/40 enzyme (Table S2).

The results revealed that compound **2** showed a high affinity for the enzymes OXA-23, OXA-48, and PDC-1, showing K_I values of 716, 131, and 11 nM, respectively. The inactivation rate of compound **2** against the latter enzymes also proved to be good, with k_{inact} values of 40, 45, and 32 ms^{-1}, respectively. A comparison with the parent compound **1** indicated that, while the inhibition efficiency (k_{inact}/K_I) of compound **2** against OXA-23 decreased by 2.5-fold compared with **1**, the opposite effect was obtained against the PDC-1 enzyme, showing a 4.6-fold increase. The latter is mainly due to a lower

https://doi.org/10.1021/acsomega.4c02984
ACS Omega 2024, 9, 26484−26494

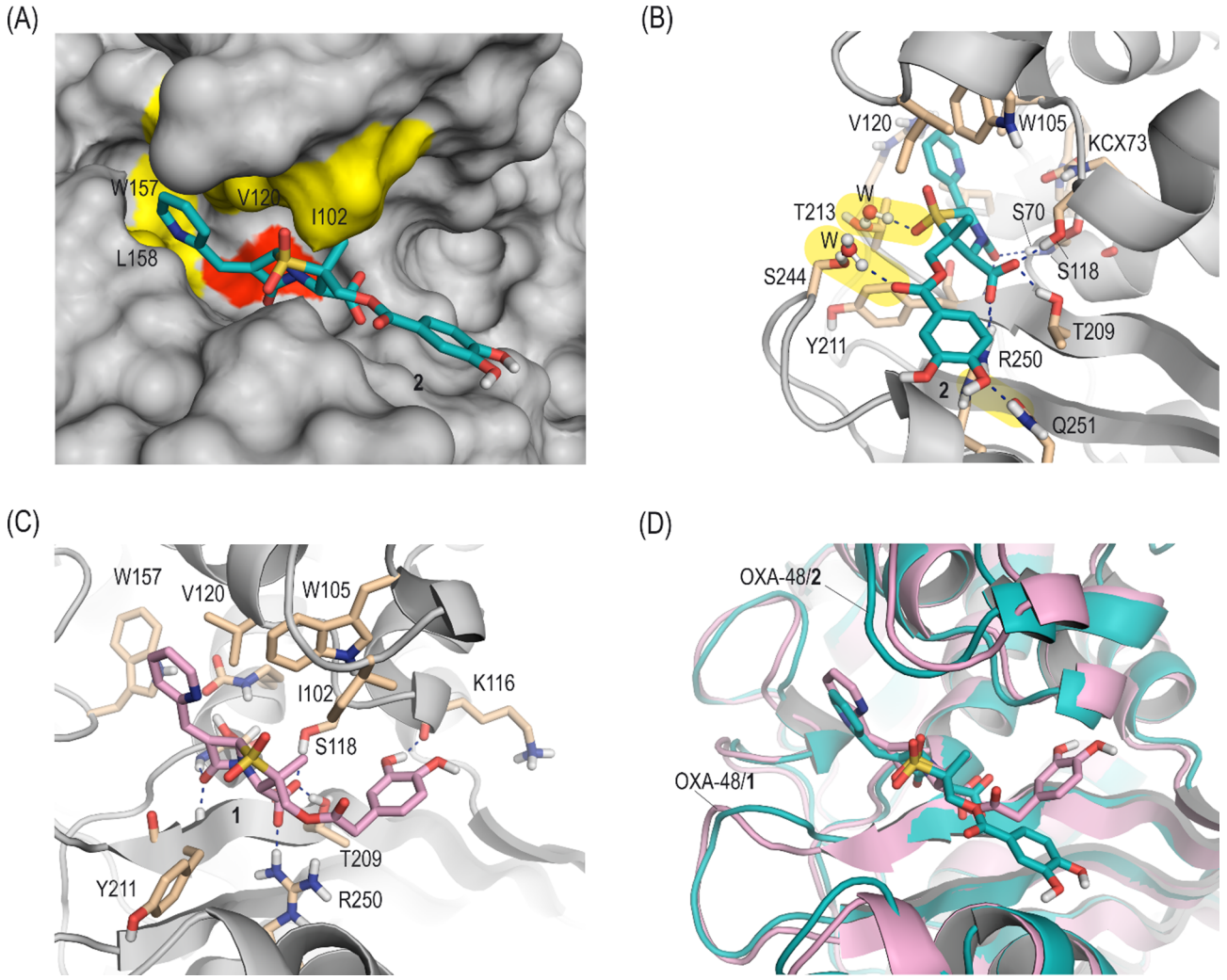

Figure 3. Binding mode of inhibitors **1** (pink) and **2** (blue) to the OXA-48 active site for the acylation reaction obtained by MD simulation studies. Snapshots taken after 30 and 80 ns of simulation, respectively, are shown. (A, B) An overall view (A) and interactions of inhibitor **2** at the active site of OXA-48 (B) are given. For the surface representation, the large hydrophobic region near the active site (yellow), which is the OXA-48 enzyme feature, and the position of the catalytic serine residue (red) are highlighted. (C) Binding mode of inhibitor **1** at the active site of OXA-48. Note how the polar contacts of the catechol, ester, and sulfonyl groups that would be promoted by ligand **2** (highlighted in yellow, panel B) would be absent for ligand **1**. (D) Superposition of the binding conformations of compounds **1** and **2** with OXA-48. Note the distinct arrangement of the side chain containing the catechol group in both ligands. Polar interactions (blue dashed lines) and relevant side-chain residues are shown and labeled.

K_I parameter, which is related to the enzyme affinity of inhibitor **2** vs **1** (113 vs 748 nM, respectively), which also occurred for the K_{iapp} value (5 vs 53 nM, respectively). For OXA-48, compound **2** was found to have a lower K_{iapp} value than the parent compound **1** (45 vs 170 nM, respectively) and a 140-fold higher inhibition efficiency than avibactam (3.4×10^5 vs 2.4×10^3 M^{-1} s^{-1}). It is important to highlight that avibactam is the best β-lactamase inhibitor approved by FDA against OXA-48.[35]

For compounds **4**–**6**, in which, like compound **2**, the iron chelator group is linked to the penicillin-based sulfone scaffold through an aromatic ester group, its inhibition efficiency against carbapenemase OXA-24/40 is shown to be similar to that of compound **1** (Table S2). Besides, this change does not seem to penalize the binding of **4**–**6** with this enzyme, and their capacity to restore imipenem antibacterial activity in vitro against *A. baumannii* strain producing OXA-24/40 is reduced by between 32- and 128-fold compared to compound **1** (MIC = 16–64 vs 0.5 μg mL^{-1}) (Table 1). These results suggested that the loss of in vitro activity would be largely due to their more limited internalization into periplasmic space.

UV–Vis Spectroscopy and Mass Spectrometry Studies. Formation of the indolizine derivative was corroborated by methanolysis of inhibitor **2**, which was the most relevant compound identified in this study. The conversion was monitored by UV–vis spectroscopy after treatment with a suspension of NaOMe in methanol at 25 °C (Figure S1). Spectra were recorded in the wavelength range between 500 and 200 nm for a 30 min period. The formation of a new band centered at 303 nm due to generation of the imine intermediate was initially observed. The intensity of the latter band rapidly decreased, and a new band centered at 393 nm appeared corresponding to the indolizine derivative, as revealed by HPLC-MS.

Binding Mode with OXA-48 and PDC-1 Enzymes. To provide a more in-depth understanding of the molecular bases responsible for the inhibitory potency obtained for compound **2** against the carbapenem-hydrolyzing class D β-lactamase

https://doi.org/10.1021/acsomega.4c02984
ACS Omega 2024, 9, 26484–26494

OXA-48 and ESBL PDC-1 enzymes, their binding mode was studied in silico. Formation of both the enzyme/ligand complexes, which triggers covalent modification of the enzyme, and the corresponding indolizine adducts was studied. To this end, docking studies were first performed using the GOLD program version 2021.3.0,[36] followed by MD simulation studies on the most plausible enzyme/ligand complexes and adducts obtained by docking to provide a more realistic picture of the target conformation upon ligand binding (induced-fit model). The enzyme coordinates of the reported crystal structure of OXA-48 inactivated by avibactam (PDB ID 4S2N,[37] 2.0 Å, chain A) and the wild-type structure of PDC-1 (PDB ID 4GZB,[38] 1.79 Å) were used for these studies. The enzyme/**2** binary complexes and the corresponding adducts obtained by docking were immersed in a truncated octahedron of TIP3P water molecules and neutralized by addition of sodium ions using the molecular mechanics force field ff14SB of AMBER 20,[39] which were then subjected to 100−200 ns of dynamic simulation following our previously reported protocol.[24]

Inactivation of OXA-48. OXA-48 has three conserved motifs I−III: STFK (I), which involves the catalytic residues S70, T71, F72 and carbamylated K73 (KCX73), SVV (II, residues S118, V119, and V120), and KTG (III, residues K208, T209, and G210).[40] The overall three-dimensional structure of OXA-48 is similar to that of the ESBL enzymes OXA-10 and OXA-13. However, it has a characteristic large hydrophobic region near the active site comprising residues W157, V120, and L158, among others, through which the enzyme fixes the carbapenem (substrate) conformation for hydrolysis. This feature, in addition with its fast hydrolysis of the adduct, would explain why its carbapenemase efficiency is quite close to that for enzymes OXA-23 and OXA-24/40, which have a unique tunnel-like entrance to also freeze the optimal carbapenem arrangement for hydrolysis.[41]

The in silico results suggest that compound **2** would be stable in the enzyme active site, as revealed by the low RMSD (root-mean-square deviation) values obtained for the enzyme backbone and ligands during the whole simulation (Figure S2). Importantly, the pyridyl moiety in compound **2** would be stabilized in the apolar region close to the reactive center via a set of favorable lipophilic interactions within the pocket (Figure 3). Compound **2** appears to be correctly arranged in the enzyme active site for reaction with the catalytic serine residue S70 by diverse hydrogen-bonding interactions with the oxyanion hole and the adjacent side-chain residues. Specifically, compound **2** is anchored to the active site via hydrogen-bonding interactions between (i) the lactam carbonyl group and the main NH groups of residues S70 and Y211 (oxyanion hole) and (ii) the carboxylate group and the side chains of residues R250, T209, and S118 (motifs II and III). These interactions proved to be strong and stable during the whole simulation since no significant changes were identified upon analysis of the variations in the relative distance between the atoms involved in them (Figure S3). Compared to compound **1**, the mobility of the side chain in **2** appears to be reduced by stronger and more stable interactions between its ester group and the residues within the pocket, which might also account for its improved efficacy. For compound **2**, the 2,3-dihydroxybenzoate moiety interacts via hydrogen-bonding with the side chains of residues Q251 (phenol groups) and S244 (ester group), the latter of which is mediated by a water molecule. These interactions were not identified in the binding mode of compound **1**, as well as the polar contact involved the sulfonyl moiety and the side chain of residue T213, which would be mediated by a water molecule (Figure 3B vs C). The impact of the length and flexibility of the linker that connects the catechol group to the penicillin-based sulfone scaffold is easily visualized by overlapping both ligand binding modes (Figure 3D). The flexibility that the presence of an extra methylene group gives to ligand **1** seems to penalize to a certain extent, anchoring it to the active center.

Simulation studies carried out on the OXA-48/**2** enzyme adduct revealed that the resulting indolizidine moiety appears to be surrounded by the apolar region close to the active site, thus further increasing its hydrophobicity and therefore hindering access of the water molecule required for hydrolysis and turnover (Figure 4). Once the indolizine adduct has formed, the presence of a positively charged chain does not seem to be a handicap as regards accommodating this moiety within the apolar region of the enzyme since this chain would be pointing toward the bulky solvent. The position of the acyl-serine adduct is fixed by several hydrogen-bonding interactions between its carboxylate group and the guanidinium group of R250 and the hydroxyl group of T209 (Figure S4). The 2,3-dihydroxybenzoate group for adduct OXA-48/**2** interacts by hydrogen-bonding with the side chains of K208 (motif III) and W222.

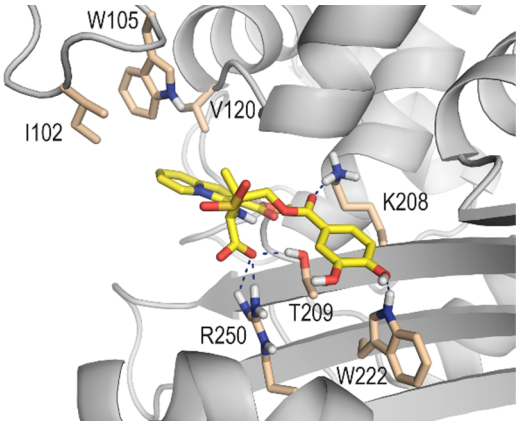

Figure 4. Overall view of the active site of enzyme OXA-48 inactivated by compound **2** (yellow) obtained by MD simulation studies. Snapshot taken after 100 ns of simulation is provided. Relevant side-chain residues are shown and labeled. Polar interactions are indicated as blue dashed lines.

Inactivation of PDC-1. The predicted binding mode of compound **2** for the chromosomal class C β-lactamase PDC-1 revealed that the β-lactam carbonyl group is anchored to the oxyanion hole via two hydrogen bonds with the main NH groups of residues S64 (essential) and S319 (Figure 5A). The pyridylalkylidene group in **2** is buried in a tunnel-like site adjacent to the catalytic serine created by folding of the H10 helix (residues 289−292) upon ligand binding. As a result, the position of the essential residue Y151 is fixed, remaining parallel to the pyridyl group in **2** due to a strong π-stacking interaction. The PDC-1/**2** complex and the interactions proved to be very stable, as revealed by the analysis of the RMSD values (protein backbone and ligands) and the relative distances between the atoms implicated during the whole simulation (Figures S5 and S6). The acyl-modified catalytic serine residue is protected from the water environment by

https://doi.org/10.1021/acsomega.4c02984
ACS Omega 2024, 9, 26484−26494

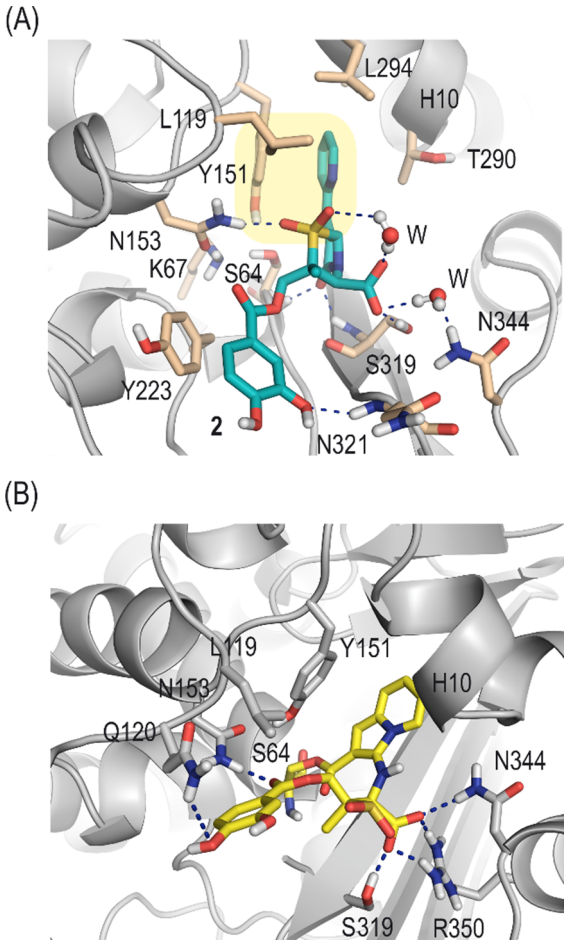

Figure 5. (A) Main interactions of inhibitor **2** (blue) in the PDC-1 active site for the acylation reaction obtained by MD simulation studies. Snapshot taken after 80 ns of simulation is shown. Polar interactions (blue dashed lines) and relevant side-chain residues are shown and labeled. Note how a parallel arrangement (yellow shadow) of the pyridine moiety in the ligand and the catalytic Y151 residue is observed for the Michaelis complex. (B) Overall view of the active site of enzyme PDC-1 inactivated by compound **2** (yellow) obtained by MD simulation studies. Snapshot taken after 90 ns of simulation is provided.

occupying the tunnel-like region generated by the H10 helix folding. The 2,3-dihydroxybenzoate moiety is located at the entrance to the active site pointing toward the bulky environment, thus resulting in a relatively flexible disposition.

The results of the simulation studies carried out on the PDC-1/**2** enzyme adduct showed that the indolizidine moiety would be embedded in the deep tunnel-like site surrounded by the inner part of the H10 helix (Figure 5B). The catechol moiety would be stabilized by the hydrogen-bonding interaction with the side chain of residue N153, while the carboxylate group would stablish strong hydrogen-bonding interactions with the guanidinium group of residue R350 and the side chains of residues S319 and N344. All these interactions showed to be stable during the whole simulation (Figure S8).

Cytotoxicity Assays. The cytotoxicity of β-lactamase inhibitor **2** in the HepG2 cell line (human hepatocellular carcinoma) was evaluated following previously reported protocols.[42] The assays were performed for triplicate using cisplatin as a control and at compound concentrations of 16 μg mL^{-1} (32.2 μM). No relevant cytotoxicity of compound **2** at the susceptibility assay concentration was identified. Thus, the % of cell growth inhibition was 7 ± 2. Under these experimental conditions, cisplatin gave a % inhibition of 60 ± 2 and an IC_{50} (μM) of 15.8 ± 1.4.

CONCLUSIONS

In summary, a series of novel 6-pyridylalkylidene penicillin-based sulfones functionalized with diverse iron chelator groups and linkages to the scaffold **1** (compounds **2**−**8**) have been designed and synthesized as β-lactamase inhibitors. The results from the in vitro studies regarding the ability of penicillin-based sulfones **2**−**8** to reinstate β-lactam antibiotic efficacy in strains carrying different types of ESBL and class D carbapenemases, along with the kinetic data with the isolated enzymes, identified compound **2** as the best inhibitor of the series. This compound, which contains a catechol group linked to the pro-*S* methyl of the sulfone scaffold via an aromatic ester, provided a β-lactamase inhibitor with an expanded spectrum of activity. Specifically, the susceptibility of ampicillin in combination with **2** against *E. coli* producing ESBL CTX-M-14 was increased. Extensive in silico studies on the formation of the Michaelis complex and adduct with the OXA-48 and PDC-1 enzymes have shown that the linkage of the catechol group via an aromatic ester appears to promote extra key interactions between the phenol and ester groups of the siderophore moiety and the residues of the active site, thus reducing the flexibility obtained with compound **1**. The results of the studies described here also suggest that the latter modification would improve its internalization into the periplasmic space.

ASSOCIATED CONTENT

Supporting Information

The Supporting Information is available free of charge at https://pubs.acs.org/doi/10.1021/acsomega.4c02984.

Details of the preparation of the reported compounds, bacterial strains and plasmids used in this study, kinetic data against OXA-24/40, UV−vis spectra and mass spectra, additional figures for the MD simulation studies, NMR spectra for compounds **2**−**8** and their synthetic intermediates, and HPLC-MS traces for compounds **2**−**8** (PDF)

Three-dimensional structures of the enzyme complex OXA-48/**2** (PDB)

Three-dimensional structure of the enzyme complex PDC-1/**2** (PDB)

Three-dimensional structure of the enzyme adduct OXA-48/**2** (PDB)

Three-dimensional structure of the enzyme adduct PDC-1/**2** (PDB)

AUTHOR INFORMATION

Corresponding Author

Concepción González-Bello − *Centro Singular de Investigación en Química Biolóxica e Materiais Moleculares (CiQUS), Departamento de Química Orgánica, Universidade de Santiago de Compostela, 15782 Santiago de Compostela, Spain;* orcid.org/0000-0001-6439-553X; Phone: (+34) 881815726; Email: concepcion.gonzalez.bello@usc.es

https://doi.org/10.1021/acsomega.4c02984
ACS Omega 2024, 9, 26484−26494

Authors

Diana Rodríguez − *Centro Singular de Investigación en Química Biolóxica e Materiais Moleculares (CiQUS), Departamento de Química Orgánica, Universidade de Santiago de Compostela, 15782 Santiago de Compostela, Spain*

Emilio Lence − *Centro Singular de Investigación en Química Biolóxica e Materiais Moleculares (CiQUS), Departamento de Química Orgánica, Universidade de Santiago de Compostela, 15782 Santiago de Compostela, Spain;* orcid.org/0000-0001-9489-9421

Juan C. Vázquez-Ucha − *Servicio de Microbiología, Complexo Hospitalario Universitario da Coruña (CHUAC), Instituto de Investigación Biomédica da Coruña (INIBIC), 15006 A Coruña, Spain*

Alejandro Beceiro − *Servicio de Microbiología, Complexo Hospitalario Universitario da Coruña (CHUAC), Instituto de Investigación Biomédica da Coruña (INIBIC), 15006 A Coruña, Spain;* orcid.org/0000-0002-6340-7815

Complete contact information is available at: https://pubs.acs.org/10.1021/acsomega.4c02984

Author Contributions

The manuscript was written with contributions from all authors. All authors have given approval to the final version of the manuscript.

Funding

This work was funded by the Spanish State Agency of Research (PID2019-105512RB-I00/AEI/10.13039/501100011033, PID2022-136963OB-I00/AEI/10.13039/501100011033, CG-B), the Xunta de Galicia [ED431C 2021/29 and Centro singular de investigación de Galicia accreditation 2024−2027 (ED431G 2023/03), CG-B], and the European Regional Development Fund (ERDF). D.R. and J.C.V.-U. thank the Xunta de Galicia for their respective predoctoral (ED481A-2016/308) and postdoctoral (IN606B-2022/009) fellowships. A.B. is grateful to the National Plan for Scientific Research, Development and Technological Innovation 2017−2020 (PI17/01482 and PI20/01212), the ISCIII-General Subdirection of Assessment and Promotion of ERDF "A way of making Europe", the CIBERINFEC (CIBER de Enfermedades Infecciosas, Instituto de Salud Carlos III), and the Galician Innovation Agency (GAIN, IN607D2021/12) for financial support.

Notes

The authors declare no competing financial interest.

TOC graphic was created by the BioRender program (www.biorender.com). The enzyme structures were analyzed and represented using the program PyMOL.[43]

■ ACKNOWLEDGMENTS

All authors are grateful to the Centro de Supercomputación de Galicia (CESGA) for use of the Finis Terrae computer.

■ DEDICATION

[§]Dedicated to the memory of Professor Sonsoles Velázquez.

■ ABBREVIATIONS

MDR, multidrug-resistant; PDC, *Pseudomonas*-derived cephalosporinase; DIAD, diisopropylazodicarboxylate; TBAI, tetrabutylammonium iodide; ESBL, extended spectrum β-lactamases; MIC, minimum inhibitory concentration; MD, molecular dynamics.

■ REFERENCES

(1) Peng, B.; Li, H.; Peng, X.-X. Call for next-generation drugs that remove the uptake barrier to combat antibiotic resistance. *Drug Discovery Today* **2023**, *28*, No. 103753.

(2) Wanted: a reward for antibiotic development *Nat. Biotechnol.* 2018, *36*, 555 .

(3) Mehrotra, T.; Konar, D.; Pragasam, A. K.; Kumar, S.; Jana, P.; Babele, P.; Paul, D.; Purohit, A.; Tanwar, S.; Bakshi, S.; Das, S.; Verma, J.; Talukdar, D.; Narendrakumar, L.; Kothidar, A.; Karmakar, S. P.; Chaudhuri, S.; Pal, S.; Jain, K.; Srikanth, C. V.; Sankar, M. J.; Atmakuri, K.; Agarwal, R.; Gaind, R.; Ballal, M.; Kammili, N.; Bhadra, R. K.; Ramamurthy, T.; Nair, G. B.; Das, B. Antimicrobial resistance heterogeneity among multidrug-resistant Gram-negative pathogens: Phenotypic, genotypic, and proteomic analysis. *Proc. Natl. Acad. Sci. U S A* **2023**, *120*, No. e2305465120.

(4) Heuretzbacher, U.; Outterson, K.; Engel, A.; Karlén, A. The global preclinical antibacterial pipeline. *Nat. Rev. Microbiol.* **2020**, *18*, 275−285.

(5) Johnston, C. W.; Badran, A. H. Natural and engineered precision antibiotics in the context of resistance. *Curr. Opin Chem. Biol.* **2022**, *69*, No. 102160.

(6) González-Bello, C.; Rodríguez, D.; Pernas, M.; Rodríguez, Á.; Colchón, E. β-Lactamase Inhibitors To Restore the Efficacy of Antibiotics against Superbugs. *J. Med. Chem.* **2020**, *63*, 1859−1881.

(7) Ayner, B.; Verderosa, A. D.; Ferro, V.; Blaskovich, M. A. T. Siderophore conjugates to combat antibiotic-resistant bacteria. *RSC Med. Chem.* **2023**, *14*, 800−822.

(8) Page, M. G. P. The role of iron and siderophores in infection, and the development of siderophore antibiotics. *Clin. Infect. Dis.* **2019**, *69* (Supplement_7), S529−S537.

(9) Rodríguez, D.; González-Bello, C. Siderophores: chemical tools for precise antibiotic delivery. *Bioorg. Med. Chem. Lett.* **2023**, *87*, No. 129282.

(10) Kramer, J.; Özkaya, Ö.; Kümmerli, R. Bacterial siderophores in community and host interactions. *Nat. Rev. Microbiol.* **2020**, *18*, 152−163.

(11) Gumienna-Kontecka, E.; Carver, P. L. Building a trojan horse: siderophore-drug conjugates for the treatment of infectious diseases. *Met. Ions Life Sci.* **2019**, *19*, 181.

(12) Bassetti, M.; Echols, R.; Matsunaga, Y.; Ariyasu, M.; Doi, Y.; Ferrer, R.; Lodise, T. P.; Naas, T.; Niki, Y.; Paterson, D. L.; Portsmouth, S.; Torre-Cisneros, J.; Toyoizumi, K.; Wunderink, R. G.; Nagata, T. D. Efficacy and safety of cefiderocol or best available therapy for the treatment of serious infections caused by carbapenem-resistant Gram-negative bacteria (CREDIBLE-CR): a randomised, open-label, multicentre, pathogen-focused, descriptive, phase 3 trial. *Lancet Infect. Dis.* **2021**, *21*, 226−240.

(13) McCreary, E. K.; Heil, E. L.; Tamma, P. D. New perspectives on antimicrobial agents: cefiderocol. *Antimicrob. Agents Chemother.* **2021**, *65*, No. e0217120.

(14) Syed, Y. Y. Cefiderocol: a review in serious gram-negative bacterial infections. *Drugs* **2021**, *81*, 1559−1571.

(15) Ong'uti, S.; Czech, M.; Robilotti, E.; Holubar, M. Cefiderocol: a new cephalosporin stratagem against multidrug-resistant gram-negative bacteria. *Clin. Infect. Dis.* **2022**, *74*, 1303−1312.

(16) Simner, P. J.; Patel, R. Cefiderocol antimicrobial susceptibility testing considerations: the achilles' heel of the trojan horse? *J. Clin Microbiol.* **2020**, *59*, e00951−20.

(17) Cordero, D. G.; Castillo-Polo, J. A.; Ruiz-Garbajosa, P.; Cantón, R. Antibacterial spectrum of cefiderocol. *Rev. Esp. Quimioter.* **2022**, *35* (Suppl 2), 20−27.

(18) Kaye, K. S.; Naas, T.; Pogue, J. M.; Rossolini, G. M. Cefiderocol, a siderophore cephalosporin, as a treatment option for infections caused by carbapenem-resistant Enterobacterales. *Infect. Dis. Ther.* **2023**, *12*, 777−806.

(19) Wang, C.; Xia, Y.; Wang, R.; Li, J.; Chan, C.-L.; Kao, R. Y.-T.; Toy, P. H.; Ho, P.-L.; Li, H.; Sun, H. Metallo-sideromycin as a dual functional complex for combating antimicrobial resistance. *Nat. Commun.* **2023**, *14*, 5311.
(20) Buynak, J. D. The discovery and development of modified penicillin- and cephalosporin-derived beta-lactamase inhibitors. *Curr. Med. Chem.* **2004**, *11*, 1951−1964.
(21) Pattanaik, P.; Bethel, C. R.; Hujer, A. M.; Hujer, K. M.; Distler, A. M.; Taracila, M.; Anderson, V. E.; Fritsche, T. R.; Jones, R. N.; Pagadala, S. R.; van den Akker, F.; Buynak, J. D.; Bonomo, R. A. Strategic design of an effective β-lactamase inhibitor: LN-1−255, A 6-alkylidene-2′-substituted penicillin sulfone. *J. Biol. Chem.* **2009**, *284*, 945−953.
(22) Buynak, J. D.; Rao, A. S.; Doppalapudi, V. R. 2-β-Substituted-6-alkylidene penicillanic acid derivatives as β-lactamase inhibitors, WO 99/33838, July 8, 1999.
(23) Rodríguez, D.; Maneiro, M.; Vázquez-Ucha, J. C.; Beceiro, A.; González-Bello, C. 6-Arylmethylidene penicillin-based sulfone inhibitors for repurposing antibiotic efficiency in priority pathogens. *J. Med. Chem.* **2020**, *63*, 3737−3755.
(24) Vázquez-Ucha, J. C.; Rodríguez, D.; Lasarte-Monterrubio, C.; Lence, E.; Arca-Suarez, J.; Maneiro, M.; Gato, E.; Perez, A.; Martínez-Guitián, M.; Juan, C.; Oliver, A.; Bou, G.; González-Bello, C.; Beceiro, A. 6-Halopyridylmethylidene penicillin-based sulfones efficiently inactivate the natural resistance of *Pseudomonas aeruginosa* to β-lactam Antibiotics. *J. Med. Chem.* **2021**, *64*, 6310−6328.
(25) Chen, Y. L.; Chang, C.-W.; Hedberg, K. Synthesis of a potent β-lactamase inhibitor-1,1-dioxo-6-(2-pyridyl)methylenepenicillanic acid and its reaction with sodium methoxide. *Tetrahedron Lett.* **1986**, *27*, 3449−3452.
(26) Bou, G.; Santillana, E.; Sheri, A.; Beceiro, A.; Sampson, J. M.; Kalp, M.; Bethel, C. R.; Distler, A. M.; Drawz, S. M.; Pagadala, S. R. R.; van den Akker, F.; Bonomo, R. A.; Romero, A.; Buynak, J. D. Design, synthesis, and crystal structures of 6-alkylidene-2′-substituted penicillanic acid sulfones as potent inhibitors of *Acinetobacter baumannii* OXA-24 carbapenemase. *J. Am. Chem. Soc.* **2010**, *132*, 13320−13331.
(27) Manna, M. S.; Tamer, Y. T.; Gaszek, I.; Poulides, N.; Ahmed, A.; Wang, X.; Toprak, F. C. R.; Woodard, D. R.; Koh, A. Y.; Williams, N. S.; Borek, D.; Atilgan, A. R.; Hulleman, J. D.; Atilgan, C.; Tambar, U.; Toprak, E. A trimethoprim derivative impedes antibiotic resistance evolution. *Nat. Commun.* **2021**, *12*, 2949.
(28) Sanderson, T. J.; Black, C. M.; Southwell, J. W.; Wilde, E. J.; Pandey, A.; Herman, R.; Thomas, G. H.; Boros, E.; Duhme-Klair, A.-K.; Routledge, A. A salmochelin S4-inspired ciprofloxacin trojan horse conjugate. *ACS Infect. Dis.* **2020**, *6*, 2532−2541.
(29) Ahmed, E.; Holmström, S. J. M. Siderophores in environmental research: roles and applications. *Microbial Biotechnol.* **2014**, *7*, 196−208.
(30) Raymond, K. N.; Allred, B. E.; Sia, A. K. Coordination chemistry of microbial iron transport. *Acc. Chem. Res.* **2015**, *48*, 2496−2505.
(31) Matlin, S. A.; Chan, L.; Catherwood, B. 6-Diazopenicillanates. part 1. reactions with furans. *J. Chem. Soc., Perkin Trans.* **1990**, *1*, 89−96.
(32) CLSI. *Performance Standards for Antimicrobial Susceptibility Testing*. CLSI supplement M100, 33rd ed.; Clinical and Laboratory Standards Institute, 2023.
(33) Vázquez-Ucha, J. C.; Maneiro, M.; Martínez-Guitián, M.; Buynak, J.; Bethel, C. R.; Bonomo, R. A.; Bou, G.; Poza, M.; González-Bello, C.; Beceiro, A. Activity of the β-lactamase inhibitor LN-1−255 against carbapenem-hydrolyzing class D β-lactamases from *Acinetobacter baumannii*. *Antimicrob. Agents Chemother.* **2017**, *61*, No. e01172-17.
(34) Vallejo, J. A.; Martínez-Guitián, M.; Vázquez-Ucha, J. C.; González-Bello, C.; Poza, M.; Buynak, J. D.; Bethel, C. R.; Bonomo, R. A.; Bou, G.; Beceiro, A. LN-1−255, a penicillanic acid sulfone able to inhibit the class D carbapenemase OXA-48. *J. Antimicrob. Chemother.* **2016**, *71*, 2171−2180.
(35) Kazmierczak, K. M.; Bradford, P. A.; Stone, G. G.; de Jonge, B. L. M.; Sahm, D. F. *In vitro* activity of ceftazidime-avibactam and aztreonam-avibactam against OXA-48-carrying Enterobacteriaceae Isolated as part of the international network for optimal resistance monitoring (INFORM) global surveillance program from 2012 to 2015. *Antimicrob. Agents Chemother.* **2018**, *62*, No. e00592.
(36) Jones, G.; Willett, P.; Glen, R. C.; Leach, A. R.; Taylor, R. Development and validation of a genetic algorithm for flexible docking. *J. Mol. Biol.* **1997**, *267*, 727−748.
(37) King, D. T.; King, A. M.; Lal, S. M.; Wright, G. D.; Strynadka, N. C. Molecular mechanism of avibactam-mediated β-lactamase inhibition. *ACS Infect. Dis.* **2015**, *1*, 175−184.
(38) Lahiri, S. D.; Mangani, S.; Durand-Reville, T.; Benvenuti, M.; Luca, F. D.; Sanyal, G.; Docquier, J.-D.; et al. Structural insight into potent broad-spectrum inhibition with reversible recyclization mechanism: avibactam in complex with CTX-M-15 and *Pseudomonas aeruginosa* AmpC β-Lactamases. *Antimicrob. Agents Chemother.* **2013**, *57*, 2496−2505.
(39) Case, D.; Cerutti, D.; Cheatham, T.; Darden, T.; Duke, R.; Giese, T.; Gohlke, H.; Goetz, A.; Greene, D.; Homeyer, N. *Amber 20 and AmberTools21*; University of California: San Francisco, 2021.
(40) Docquier, J.-D.; Calderone, V.; De Luca, F.; Benvenuti, M.; Giuliani, F.; Bellucci, L.; Tafi, A.; Nordmann, P.; Botta, M.; Rossolini, G. M.; Mangani, S. Crystal Structure of the OXA-48 β-lactamase reveals mechanistic diversity among class D carbapenemases. *Chem. Biol.* **2009**, *16*, 540−547.
(41) Stojanoski, V.; Hu, L.; Sankaran, B.; Wang, F.; Tao, P.; Prasad, B. V. V.; Palzkill, T. Mechanistic basis of OXA-48-like β-lactamases' hydrolysis of carbapenems. *ACS Infect. Dis.* **2021**, *7*, 445−460.
(42) Panciera, M.; Lence, E.; Rodríguez, A.; Gracia, B.; Aínsa, J. A.; Marco-Marín, C.; Rubio, V.; Duarte Correia, C. R.; González-Bello, C. Discovery of 3H-pyrrolo[2,3-*c*]quinolines with activity against *Mycobacterium tuberculosis* by allosteric inhibition of the glutamate-5-kinase enzyme. *Eur. J. Med. Chem.* **2022**, *232*, No. 114206.
(43) DeLano, W. L. *The PyMOL Molecular Graphics System*; DeLano Scientific LLC: Palo Alto, CA, 2008. http://www.pymol.org/ (accessed 19 March 2024).

https://doi.org/10.1021/acsomega.4c02984
ACS Omega 2024, 9, 26484−26494